How to cite: *Angew. Chem. Int. Ed.* **2021**, *60*, 13641–13646
International Edition: doi.org/10.1002/anie.202101187
German Edition: doi.org/10.1002/ange.202101187

Solid Electrolytes

Polymorphism and Fast Potassium-Ion Conduction in the T5 Supertetrahedral Phosphidosilicate KSi_2P_3

*Arthur Haffner[+], Anna-Katharina Hatz[+], Otto E. O. Zeman, Constantin Hoch, Bettina V. Lotsch, and Dirk Johrendt**

Dedicated to Professor Peter Klüfers on the occasion of his 70th birthday

Abstract: *The all-solid-state battery (ASSB) is a promising candidate for electrochemical energy storage. In view of the limited availability of lithium, however, alternative systems based on earth-abundant and inexpensive elements are urgently sought. Besides well-studied sodium compounds, potassium-based systems offer the advantage of low cost and a large electrochemical window, but are hardly explored. Here we report the synthesis and crystal structure of K-ion conducting T5 KSi_2P_3 inspired by recent discoveries of fast ion conductors in alkaline phosphidosilicates. KSi_2P_3 is composed of SiP_4 tetrahedra forming interpenetrating networks of large T5 supertetrahedra. The compound passes through a reconstructive phase transition from the known T3 to the new tetragonal T5 polymorph at 1020 °C with enantiotropic displacive phase transitions upon cooling at about 155 °C and 80 °C. The potassium ions are located in large channels between the T5 supertetrahedral networks and show facile movement through the structure. The bulk ionic conductivity is up to 2.6×10^{-4} S cm^{-1} at 25 °C with an average activation energy of 0.20 eV. This is remarkably high for a potassium ion conductor at room temperature, and marks KSi_2P_3 as the first non-oxide solid potassium ion conductor.*

All-solid-state batteries (ASSB) with solid instead of liquid electrolytes are considered as the next generation energy storage devices because they provide higher energy densities and faster charging rates than conventional systems.[1–6] For the development of ASSBs, the solid electrolyte is a critical component and its ionic conductivity a key performance indicator. So far, several lithium ion-conducting materials are well investigated. Garnets such as doped $Li_7La_3Zr_2O_{12}$ and $Li_{1.4}Al_{0.4}Ti_{1.6}(PO_4)_3$ exhibit bulk ionic conductivities up to 10^{-3} S cm^{-1} at room temperature. Similar and even higher lithium ion conductivities in the range of 1.6×10^{-4} to 2.5×10^{-2} S cm^{-1} were found in ternary lithium thiophosphates,[7] halide argyrodites,[8,9] $Li_{10}GeP_2S_{12}$-type materials[10] and rare-earth halides.[11–13] Recently, it became apparent that phosphidosilicates may be promising candidates for solid electrolytes. These compounds contain SiP_4 tetrahedra, which are isolated in Li_8SiP_4,[14] while in $Li_{10}Si_2P_6$ or $Li_3Si_3P_7$[15] the tetrahedra are condensed via edges or vertices to reduce the charge. The SiP_4 tetrahedra in Li_2SiP_2 form interpenetrating networks of T2 supertetrahedra,[14] while in $LiSi_2P_3$ fused T4 and T5 entities are present.[16] The lithium ion conductivities are between 4×10^{-7} S cm^{-1} (Li_2SiP_2)[14] and 1×10^{-3} S cm^{-1} ($Li_{14}SiP_6$)[17] with activation energies of 0.49 to 0.30 eV, respectively. NMR data of $LiSi_2P_3$ reveal an activation energy of about 0.1 eV indicating an even more facile ion transport in this compound. However, lithium batteries for large scale applications are restricted by the availability and cost of lithium.[18–22] Therefore, systems with earth abundant cheap alternatives such as sodium or potassium are requested. Solid sodium electrolytes like Na_3PS_4[23] or NaSICON-type $Na_{3.4}Sc_2(SiO_4)_{0.4}(PO_4)_{2.6}$[24,25] have conductivities on the order of 2×10^{-4} S cm^{-1} and 7×10^{-4} S cm^{-1}, respectively. β-Alumina,[26] Na_3SbS_4[27,28] or $Na_{11}Sn_2PS_{12}$[29,30] exceed these conductivities by about one order of magnitude. The phosphidosilicates $Na_{23}Si_{9n+19}P_{12n+33}$ based on interpenetrating networks of fused T3 to T5 supertetrahedra turned out to be competitive.[31] *HT*-$NaSi_2P_3$ exhibits solely T5 entities and shows a total sodium ion conductivity of 4×10^{-4} S cm^{-1} with a low activation energy (E_a) of 0.25 eV. NMR data reveal an even lower activation energy of 0.11 eV, suggesting a facile Na hopping process. While sodium is much more abundant than lithium, it has a less negative electrode potential (−2.71 V) compared to lithium (−3.04 V). In contrast, potassium has a lower potential than Na (−2.93 V) that enables an improved cell output voltage.

Since the availability and low cost of potassium are comparable with those of sodium, the exploration of potassium ion batteries (KIBs) appears promising. So far, studies on KIBs employing potassium metal anodes, solid electrolytes and cathodes such as Prussian blue with remarkable capacities and cycling stabilities were reported.[32–35] Surprisingly, only a few solid potassium ion electrolytes are known

[*] M. Sc. A. Haffner,[+] M. Sc. O. E. O. Zeman, Dr. C. Hoch, Prof. Dr. D. Johrendt
Department of Chemistry, Ludwig Maximilian University of Munich
Butenandtstrasse 5–13 (D), 81377 Munich (Germany)
E-mail: johrendt@lmu.de
M. Sc. A.-K. Hatz,[+] Prof. Dr. B. V. Lotsch
Department of Nanochemistry, Max Plank Institute for Solid State Research
Heisenbergstrasse 1, 70569 Stuttgart (Germany)
[+] These authors contributed equally to this work.
Supporting information and the ORCID identification number(s) for the author(s) of this article can be found under: https://doi.org/10.1002/anie.202101187.

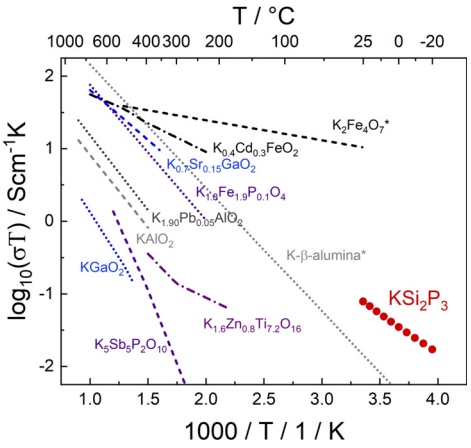

Figure 1. K^+-ion conductivities of known materials and of KSi_2P_3-*mC*928 (sample 2c in Table S9). Asterisks indicate single-crystal data. References and activation energies are in Table S8.

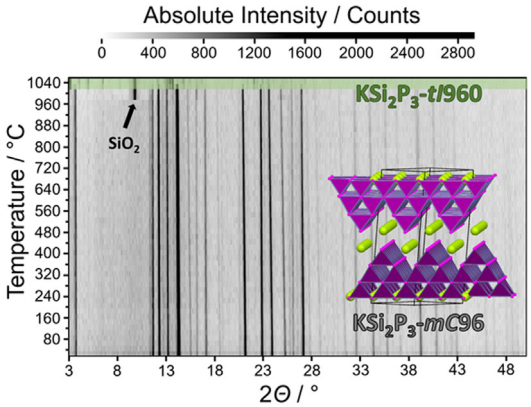

Figure 2. High temperature Mo-Kα_1 X-ray powder diffraction pattern of a KSi_2P_3-*mC*96 sample with a phase transition to KSi_2P_3-*tI*960 at about 1020 °C (highlighted in green). Inset shows the crystal structure of the known KSi_2P_3-*mC*96 compound.

(Figure 1, for data and references see Table S8). These materials are oxides and show conductivities in a reasonable range for applications (10^{-4}–10^{-2} S cm^{-1}) only at high temperatures of 300–400 °C. The only exception is polycrystalline $K_2Fe_4O_7$ with a conductivity of 5×10^{-2} S cm^{-1} at room temperature. However, single crystal impedance spectroscopy shows that the potassium ion migration in this compound is predominantly two-dimensional.[34]

In this work, we address the family of potassium phosphidosilicates as possible solid electrolytes. Currently only the compounds K_2SiP_2[36] and the layered T3 KSi_2P_3[37] are known in this system. Both are not promising as ion conductors because of the lack of partial occupied potassium sites. Here we report three new polymorphs of KSi_2P_3 with T5 supertetrahedral structures related to the sodium ion conductor $NaSi_2P_3$.[31] The polymorphs are characterized by X-ray powder diffraction based on the single-crystal data of the high temperature polymorph. Electrochemical impedance and MAS-NMR spectra of the new monoclinic modification revealed a remarkably high σ_{bulk} (K^+) up to 2.6×10^{-4} S cm^{-1} at 25 °C, and a low activation energy of 0.20 eV. This material hence qualifies as the first non-oxide fast solid potassium ion conductor.

KSi_2P_3 with the space group *C*2/*c* was first described by Feng et al.[37] and is denominated as KSi_2P_3-*mC*96 in the following. It contains SiP_4 tetrahedra which form T3 supertetrahedra according to the Yaghi nomenclature.[38] These T3 entities are fused by one common SiP_4 tetrahedron resulting in a layered structure with the K^+ ions located on two fully occupied general Wyckoff sites between T3 supertetrahedral layers (see inset of Figure 2). This structure is stable up to 1000 °C.

We find a mixture of two phases at 1020 °C before KSi_2P_3-*mC*96 is completely transformed to a tetragonal modification at 1040 °C, denoted as KSi_2P_3-*tI*960. Figure 2 shows the high temperature diffraction patterns. The additional reflection at about 9.8° indicates crystallization of the silica capillary. We were able to solve and refine the structure of this metastable high temperature polymorph quenched to room temperature with single-crystals. For details we refer to the experimental section in the Supporting Information). Table 1 summarizes the single-crystal data of KSi_2P_3-*tI*960 in space group $I4_1/acd$ (No. 142).[39] Atom positions and displacement factors are given in Tables S1 and S2 of the Supporting Information. KSi_2P_3-*tI*960 is also built from SiP_4 tetrahedra, but now forming three-dimensional networks of T5 supertetrahedra as shown in Figure 3. Every T5 cluster has a missing silicon site in its center, affecting the adjacent four phosphorus atoms by shifting them slightly towards the vacancy. This leads to shorter average P-P distances of 3.2 Å compared to 3.7 Å of the phosphorus atoms not neighboring the missing site. This appears counter-intuitive but has been already observed in several T5 supertetrahedral compounds, such as B_2S_3,[40] $LiSi_2P_3$,[16] *HT*- and *LT*-$NaSi_2P_3$[31] or UCR-15.[41] A possible explanation could be the preservation of charge neutrality in the interior of the T5 entity, since the T5 cluster is a section of the sphalerite-type structure with silicon defects resulting in the sum formula of Si_3P_4. However, this binary compound has

Table 1: Single crystal data of the high temperature polymorph KSi_2P_3-*tI*960 measured at 25 °C.

Formula	KSi_2P_3-*tI*960
space group	$I4_1/acd$ (No. 142)
a /Å	21.922(2)
c /Å	39.868(3)
V_{cell} /Å^3	19160(3)
Z	128
$\rho_{X\text{-}ray}$ /(g cm^{-3})	2.088
λ /Å	0.71073 (Mo-Kα)
μ /mm^{-1}	1.937
Θ-range /°	2.120–30.586
reflections measured	459701
independent reflections	7358
parameters	283
R_σ	0.0095
R_{int}	0.0452
R_1 ($F^2>2\sigma(F^2)$)/all	0.0391/ 0.0438
wR_2 ($F^2>2\sigma(F^2)$)/all	0.0919/ 0.0951
Goof	1.102
restraints	1
$\Delta\rho_{max/min}$ /(e Å^{-3})	+1.610/ −1.374

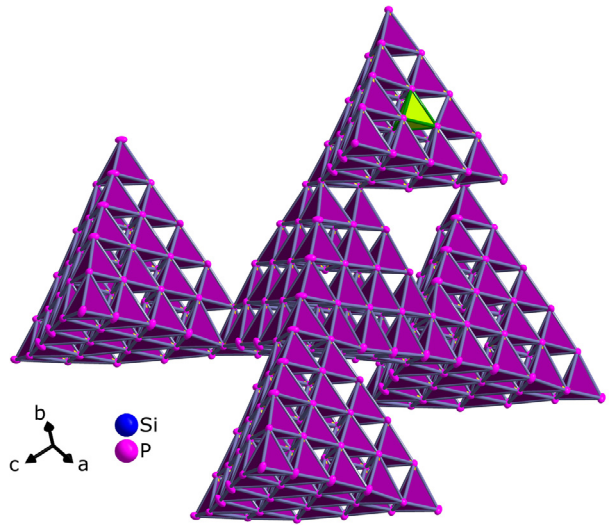

Figure 3. Three-dimensional fused T5 supertetrahedra composed of SiP_4 tetrahedra in KSi_2P_3-*tI*960. Every T5 cluster lacks one central silicon atom indicated by the green empty tetrahedron in the upper T5 cluster, where one layer of SiP_4 tetrahedra was removed for clarity.

not been confirmed experimentally, but predicted by DFT calculations.[42,43] The T5 clusters share one common SiP_4 tetrahedron resulting in a three-dimensional anionic network with giant voids interpenetrated by a second crystallographically equivalent network. These can be ascribed hierarchically to a diamond type network, resembling the structure of homeotypic *HT*-$NaSi_2P_3$.[31]

The potassium ions reside in big cavities of the supertetrahedral networks with large displacement factors and an average occupancy of 0.4. All eleven potassium positions are partially occupied and thus disordered (see Figure 4), similar

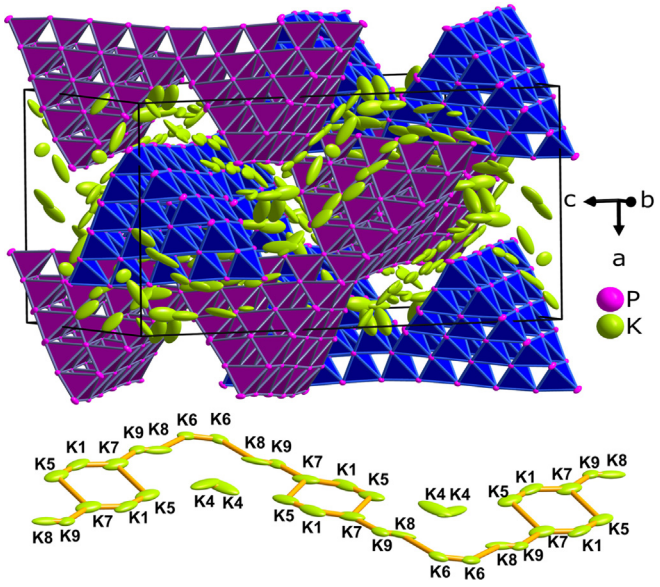

Figure 4. Unit cell of KSi_2P_3-*tI*960 with large displacements of the K ions (top, ellipsoids with 90% probability) and K positions in the voids along [111] indicating a possible ion migration pathway (bottom, ellipsoids with 50% probability).

to *HT*-$NaSi_2P_3$, which indicates mobility of potassium ions already at room temperature.

KSi_2P_3-*tI*960 goes through displacive phase transitions upon cooling. As shown in Figure 5, KSi_2P_3-*tI*960 exhibits a splitting of the most intense reflections at a diffraction angle range of 13.1 to 13.7° (Mo-Kα_1) at 155 °C. Two of these split reflections approach each other while the third moves

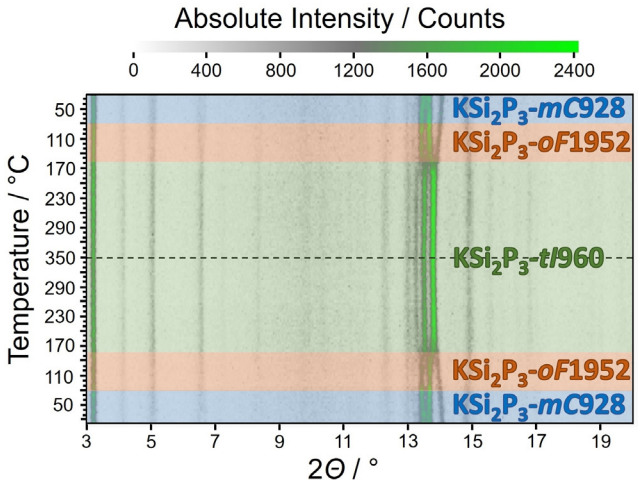

Figure 5. High temperature X-ray powder diffraction (Mo-Kα_1) of a KSi_2P_3-*mC*928 sample upon heating to 350 °C and subsequent cooling. KSi_2P_3-*mC*928 (highlighted in blue) transforms at 80 °C to KSi_2P_3-*oF*1952 (orange), before a further phase transition at 155 °C yields KSi_2P_3-*tI*960 (green). The T5 compound is enantiotropic.

towards a higher angle of about 14° beginning at 80 °C, indicating a third phase transition. These phase transitions occur upon heating and cooling of a KSi_2P_3 sample making this T5 compound enantiotropic (see Figure 5). We were not able to synthesize suitable single-crystals of the two low temperature modifications mainly due to twinning. Therefore, we stabilized the different modifications for powder diffraction analysis at ambient conditions. While the room temperature modification is easily producible with conventional solid-state methods, small amounts of the other modification could only be obtained by a modified synthesis as described in the Supporting Information. The Cu-Kα_1 diffraction patterns and Rietveld fits of the respective modifications are shown in Figure 6 (enlarged in the SI Figures S1–3) highlighting their most prominent differences consisting in the splitting, the intensity distribution, and the shifting towards higher diffraction angles of the indicated reflections. Acceptable refinements were obtained by *translationsgleiche* (*t*2) symmetry reductions from tetragonal KSi_2P_3-*tI*960 (space group $I4_1/acd$) to the orthorhombic and monoclinic subgroups of KSi_2P_3-*oF*1952 (*Fddd*) and KSi_2P_3-*mC*928 (*C*2/*c*).

The potassium positions were calculated from the symmetry reduced single-crystal structure data of KSi_2P_3-*tI*960. Therefore, these positions do not strictly follow the *Bärnighausen tree* while silicon and phosphorus do. The displacive phase transitions are mainly contractions of the crystal structure as visible in Table 2, thus increasing the crystallo-

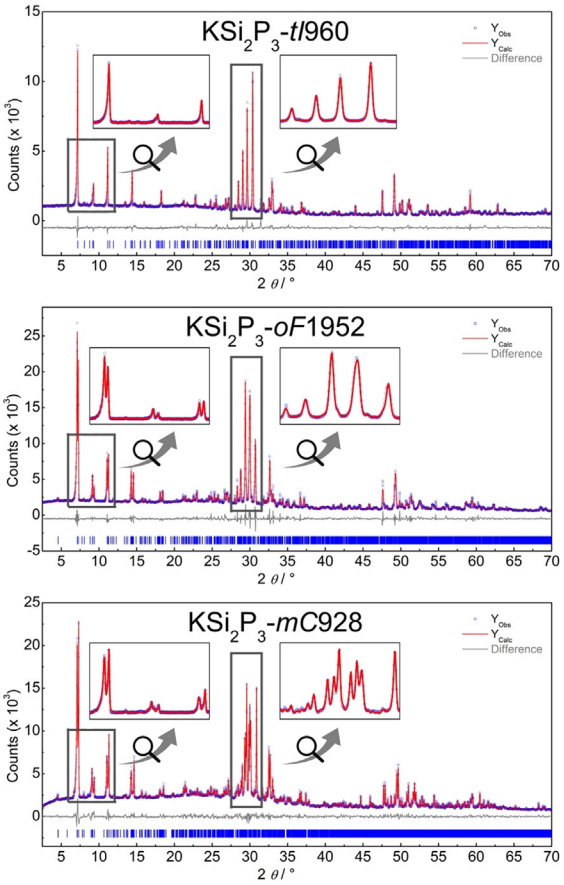

Figure 6. X-ray powder diffraction patterns (Cu-Kα_1) of tetragonal (top), orthorhombic (middle) and monoclinic (bottom) KSi_2P_3.

Table 2: Rietveld refinement results of the T5 KSi_2P_3 modifications.

Modification	Ksi_2P_3-*tI*960	KSi_2P_3-*oF*1952	KSi_2P_3-*mC*928
space group	$I4_1/acd$ (No. 142)	*Fddd* (No. 70)	*C*2/*c* (No. 15)
a /Å	21.8826(3)	31.529(1)	31.8337(4)
b /Å	21.8826(3)	30.5475(5)	30.4796(3)
c /Å	40.2923(8)	39.961(1)	25.2909(2)
β /°	90	90	128.7029(8)
V_{cell} /Å^3	19293.8(6)	38487(2)	19150.3(4)
$\rho_{X\text{-ray}}$ /(g cm^{-3})	2.07651(6)	2.0842(1)	2.11092(5)

graphic density along with the symmetry reduction (note that the cell parameters given in Table 2 appear dissimilar due to different space groups).

We have confirmed the composition and structure model of KSi_2P_3-*mC*928 with EDX (Figure S4, Table S7) and MAS-NMR measurements. The ^{29}Si spectrum (Figure S5) has broad signals between $\delta(^{29}\text{Si}) = -12$ to -26 ppm originating from 32 crystallographically inequivalent silicon atoms on general Wyckoff sites. Since the structure of KSi_2P_3-*mC*928 is homeotypic to *HT*-$NaSi_2P_3$, the ^{31}P spectra are comparable as shown in Figure 7. KSi_2P_3-*mC*928 exhibits four broad signals within almost the same chemical shift range compared to the tetragonal sodium phase. Integration of these signals in the KSi_2P_3-*mC*928 spectrum yields the same intensity distribution of 4:4:3:1 as in *HT*-$NaSi_2P_3$.[31]

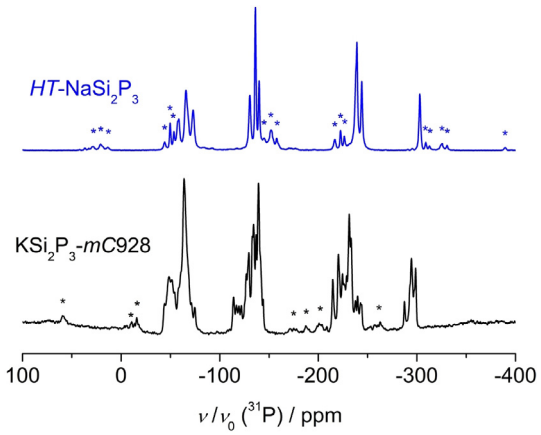

Figure 7. Normalized ^{31}P MAS NMR spectra of *HT*-$NaSi_2P_3$ (top, blue) and KSi_2P_3-*mC*928 (bottom, black) at 25 kHz and a magnetic field $B_0 = 11.7$ T. Asterisks indicate rotational side bands.

The resonance pattern of KSi_2P_3-*mC*928 is more complicated than that of *HT*-$NaSi_2P_3$ due to the symmetry reduction from tetragonal to monoclinic, which leads to splitting of all resonances and impeding a simple intensity assignment to the respective phosphorus atoms. Assuming that the upfield signal at $\delta(^{31}\text{P}) = -298.7$ ppm is the result of only one phosphorus atom, a sectional intensity integration of the whole spectrum is possible. It results in 49 distinct atoms being very close to the number of 48 atoms as predicted by X-ray diffraction. Hence, the NMR measurements are in line with the crystal structure.

We have identified possible migration pathways of all polymorphs of KSi_2P_3 from geometrical calculations yielding four large channels through the structure, which are connected by short passages along every supertetrahedral face. This indicates a 3D ion conduction similar to $NaSi_2P_3$. The calculated migration paths are visualized in Figure S6–S8 in the Supporting Information.

We have shown recently that ionic conductivity in supertetrahedral phosphidosilicates increases with increasing cluster size.[31] In view of the T5 structure of KSi_2P_3, high K-ion mobility seems more likely than in the T3 structure. We applied electrochemical impedance spectroscopy (EIS) and potentiostatic polarization measurements as described in the SI on several samples from different batches to assess the ionic and electronic conductivity. All results are listed in Table S9 and S10, and a representative impedance spectrum at -20 °C (sample 2b in Table S9) is shown in Figure 8. The measurements were performed at low temperatures to deconvolute the bulk properties of the material and to avoid phase changes that already occur at 80 °C, which may influence the performance. The spectrum contains high and low frequency contributions followed by a spike resulting from the polarization of K^+ ions at the blocking electrodes at low frequencies. The spectrum is fitted with the equivalent circuit model depicted in the inset in Figure 8. For the high frequency semicircle modelled by R1-CPE1, an effective capacitance $C_{\text{eff}} = (Q/(R^{\alpha-1}))^{1/\alpha}$ of 8 pF is calculated that corresponds to a relative permittivity of 24. This is a typical value for the bulk contributions of a solid inorganic mate-

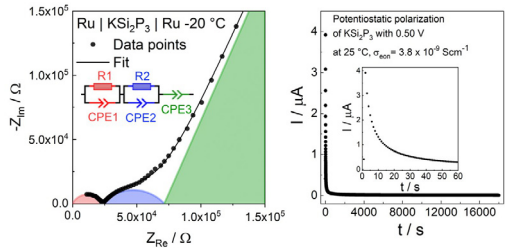

Figure 8. Left: Impedance spectra of KSi_2P_3 at −20 °C (sample 6 in Table S9), fitted with the equivalent circuit model shown in the inset. The spectrum can be deconvoluted into bulk (high frequency semicircle R1CPE1) and surface/interlayer contributions (low frequency semicircle). Right: Potentiostatic polarization curve over 5 h showing a low electronic conductivity of 3.8×10^{-9} S cm^{-1}. Inset shows data at short times.

rial.[44] The low frequency semicircle (R2-CPE2) possesses a much larger C_{eff} of 9×10^{-7} F, thus it presumably stems from grain boundaries or a surface layer.[44] The low frequency semicircle CPE3 models the polarization of ions at the electrode. The measured ionic conductivities σ_{bulk} (K^+) of nine samples from three batches (cf. Table S9) are between 0.13×10^{-4} and 2.6×10^{-4} S cm^{-1} with an average activation energy of 0.20 ± 0.04 eV. The scatter of conductivities is typical for a solid ion conductor as previously revealed in a round robin study of sulfide electrolytes,[45] and can be rationalized by batch-to-batch variations as well as differences in pellet preparation, annealing and sputtering of each sample. The highest bulk conductivity we found is 2.6×10^{-4} S cm^{-1} at room temperature with an activation energy of 0.21 eV (plotted in Figure S9), which is consistent with the averaged activation energy of the high frequency semicircle of all samples (0.20 ± 0.04 eV). This result is directly compared to literature data in Figure 1, highlighting its uniqueness as first non-oxide K ion conductor with high ionic conductivity at room temperature and below (down to −20 °C) and a low activation energy, indicating facile ion migration within the large channels of the structure. KSi_2P_3 exhibits an even higher ionic conductivity than K-β-Alumina single-crystals. Compared to other potassium ion conductors, KSi_2P_3 contains neither redox active transition metals nor expensive or rare elements.

The measured total ionic conductivity ranges from 0.045×10^{-4} to 2.0×10^{-4} S cm^{-1} and can be calculated from R_{tot} as sum of R1 + R2 with $\sigma_{tot}=d/(A\cdot R_{tot})$ with d being the thickness and A the area of the sample. This shows that even the total ionic conductivity is reasonably fast for an ionic conductor at room temperature. The activation energy of the low frequency semicircle (R2-CPE2) of 0.19 ± 0.03 eV resembles the activation energy of the bulk process (also cf. Figure S9). Thus, there is no indication of the presence of highly resistive grain boundaries. The similar activation energy rather points to a current constriction phenomenon that could result from a limited contact area between the grains, which is consistent with the low geometrical density of 77 ± 3 % of the sample pellets.[46] Therefore, by optimizing the sample preparation and microstructure, the total conductivity may be enhanced further.

The partial electronic conductivity was measured by a potentiostatic polarization experiment over several hours at 0.25 and 0.5 V for several samples (cf. Table S10). A representative plot is shown in Figure 8 (right). The electronic conductivity ranges from 0.09×10^{-8} to 1.1×10^{-8} S cm^{-1}, resulting in a transference number $\tau_i=\sigma_{ion}/(\sigma_{ion}+\sigma_{eon})$ of 0.9998. This suggests that this material can be classified as a predominantly ionic conductor.

In summary, we have identified three new polymorphs of KSi_2P_3 with T5 supertetrahedra and K^+-ion conductivities up to 2.6×10^{-4} S cm^{-1} at 25 °C. The hitherto known modification consists of T3 supertetrahedra without partially occupied K sites, which hampers ion conduction. We demonstrate fast potassium ion conduction through three-dimensional connected voids between large T5 supertetrahedra. KSi_2P_3 contains low cost, non-redox active and abundant elements. As the first non-oxide solid material, KSi_2P_3 extents the compositional space of solid potassium ion conductors, which is key for the rational design of further potassium solid electrolytes. Further investigations must show whether these compounds are suitable for use in batteries.

Acknowledgements

We thank Dr. Peter Mayer for help with crystallography, and the Deutsche Forschungsgemeinschaft (DFG) as well as the German Federal Ministry of Research and Education (BMBF), project 03XP0177B (FestBatt), for financial support. Open access funding enabled and organized by Projekt DEAL.

Conflict of interest

The authors declare no conflict of interest.

Keywords: ion conductivity · phosphidosilicate · potassium · solid electrolyte · supertetrahedra

[1] M. Armand, J. M. Tarascon, *Nature* **2008**, *451*, 652–657.
[2] J. C. Bachman, S. Muy, A. Grimaud, H. H. Chang, N. Pour, S. F. Lux, O. Paschos, F. Maglia, S. Lupart, P. Lamp, L. Giordano, Y. Shao-Horn, *Chem. Rev.* **2016**, *116*, 140–162.
[3] Y. Wang, S. Song, C. Xu, N. Hu, J. Molenda, L. Lu, *Nano Mater. Sci.* **2019**, *1*, 91–100.
[4] Z. Zhang, Y. Shao, B. Lotsch, Y.-S. Hu, H. Li, J. Janek, L. F. Nazar, C.-W. Nan, J. Maier, M. Armand, L. Chen, *Energy Environ. Sci.* **2018**, *11*, 1945–1976.
[5] R. Chen, W. Qu, X. Guo, L. Li, F. Wu, *Mater. Horiz.* **2016**, *3*, 487–516.
[6] Y.-G. Lee, S. Fujiki, C. Jung, N. Suzuki, N. Yashiro, R. Omoda, D.-S. Ko, T. Shiratsuchi, T. Sugimoto, S. Ryu, J. H. Ku, T. Watanabe, Y. Park, Y. Aihara, D. Im, I. T. Han, *Nat. Energy* **2020**, *5*, 299–308.
[7] Z. Liu, W. Fu, E. A. Payzant, X. Yu, Z. Wu, N. J. Dudney, J. Kiggans, K. Hong, A. J. Rondinone, C. Liang, *J. Am. Chem. Soc.* **2013**, *135*, 975–978.
[8] M. A. Kraft, S. P. Culver, M. Calderon, F. Böcher, T. Krauskopf, A. Senyshyn, C. Dietrich, A. Zevalkink, J. Janek, W. G. Zeier, *J. Am. Chem. Soc.* **2017**, *139*, 10909–10918.

[9] M. A. Kraft, S. Ohno, T. Zinkevich, R. Koerver, S. P. Culver, T. Fuchs, A. Senyshyn, S. Indris, B. J. Morgan, W. G. Zeier, *J. Am. Chem. Soc.* **2018**, *140*, 16330 – 16339.
[10] N. Kamaya, K. Homma, Y. Yamakawa, M. Hirayama, R. Kanno, M. Yonemura, T. Kamiyama, Y. Kato, S. Hama, K. Kawamoto, A. Mitsui, *Nat. Mater.* **2011**, *10*, 682 – 686.
[11] X. Li, J. Liang, J. Luo, M. Norouzi Banis, C. Wang, W. Li, S. Deng, C. Yu, F. Zhao, Y. Hu, T.-K. Sham, L. Zhang, S. Zhao, S. Lu, H. Huang, R. Li, K. R. Adair, X. Sun, *Energy Environ. Sci.* **2019**, *12*, 2665 – 2671.
[12] H.-J. Steiner, H. D. Lutz, *Z. Anorg. Allg. Chem.* **1992**, *613*, 26 – 30.
[13] T. Asano, A. Sakai, S. Ouchi, M. Sakaida, A. Miyazaki, S. Hasegawa, *Adv. Mater.* **2018**, *30*, 1803075.
[14] L. Toffoletti, H. Kirchhain, J. Landesfeind, W. Klein, L. van Wüllen, H. A. Gasteiger, T. F. Fässler, *Chem. Eur. J.* **2016**, *22*, 17635 – 17645.
[15] H. Eickhoff, L. Toffoletti, W. Klein, G. Raudaschl-Sieber, T. F. Fässler, *Inorg. Chem.* **2017**, *56*, 6688 – 6694.
[16] A. Haffner, T. Bräuniger, D. Johrendt, *Angew. Chem. Int. Ed.* **2016**, *55*, 13585 – 13588; *Angew. Chem.* **2016**, *128*, 13783 – 13786.
[17] S. Strangmüller, H. Eickhoff, D. Müller, W. Klein, G. Raudaschl-Sieber, H. Kirchhain, C. Sedlmeier, V. Baran, A. Senyshyn, V. L. Deringer, L. van Wüllen, H. A. Gasteiger, T. F. Fässler, *J. Am. Chem. Soc.* **2019**, *141*, 14200 – 14209.
[18] K. Vignarooban, R. Kushagra, A. Elango, P. Badami, B. E. Mellander, X. Xu, T. G. Tucker, C. Nam, A. M. Kannan, *Int. J. Hydrogen Energy* **2016**, *41*, 2829 – 2846.
[19] M. Sawicki, L. L. Shaw, *RSC Adv.* **2015**, *5*, 53129 – 53154.
[20] N. Yabuuchi, K. Kubota, M. Dahbi, S. Komaba, *Chem. Rev.* **2014**, *114*, 11636 – 11682.
[21] H. Pan, Y.-S. Hu, L. Chen, *Energy Environ. Sci.* **2013**, *6*, 2338 – 2360.
[22] H. Vikström, S. Davidsson, M. Höök, *Appl. Energy* **2013**, *110*, 252 – 266.
[23] A. Hayashi, K. Noi, A. Sakuda, M. Tatsumisago, *Nat. Commun.* **2012**, *3*, 856.
[24] M. Kaus, M. Guin, M. Yavuz, M. Knapp, F. Tietz, O. Guillon, H. Ehrenberg, S. Indris, *J. Phys. Chem. C* **2017**, *121*, 1449 – 1454.
[25] M. Guin, F. Tietz, O. Guillon, *Solid State Ionics* **2016**, *293*, 18 – 26.
[26] A. Hooper, *J. Phys. D* **1977**, *10*, 1487 – 1496.
[27] L. Zhang, D. Zhang, K. Yang, X. Yan, L. Wang, J. Mi, B. Xu, Y. Li, *Adv. Sci.* **2016**, *3*, 1600089.
[28] A. Hayashi, N. Masuzawa, S. Yubuchi, F. Tsuji, C. Hotehama, A. Sakuda, M. Tatsumisago, *Nat. Commun.* **2019**, *10*, 5266.
[29] Z. Zhang, E. Ramos, F. Lalère, A. Assoud, K. Kaup, P. Hartman, L. F. Nazar, *Energy Environ. Sci.* **2018**, *11*, 87 – 93.
[30] M. Duchardt, U. Ruschewitz, S. Adams, S. Dehnen, B. Roling, *Angew. Chem. Int. Ed.* **2018**, *57*, 1351 – 1355; *Angew. Chem.* **2018**, *130*, 1365 – 1369.
[31] A. Haffner, A.-K. Hatz, I. Moudrakovski, B. V. Lotsch, D. Johrendt, *Angew. Chem. Int. Ed.* **2018**, *57*, 6155 – 6160; *Angew. Chem.* **2018**, *130*, 6263 – 6268.
[32] S. Komaba, T. Hasegawa, M. Dahbi, K. Kubota, *Electrochem. Commun.* **2015**, *60*, 172 – 175.
[33] J. C. Pramudita, D. Sehrawat, D. Goonetilleke, N. Sharma, *Adv. Energy Mater.* **2017**, *7*, 1602911.
[34] H. Yuan, H. Li, T. Zhang, G. Li, T. He, F. Du, S. Feng, *J. Mater. Chem. A* **2018**, *6*, 8413 – 8418.
[35] A. Eftekhari, *J. Power Sources* **2004**, *126*, 221 – 228.
[36] B. Eisenmann, M. Somer, *Z. Naturforsch. B* **1984**, *39*, 736 – 738.
[37] K. Feng, L. Kang, W. Yin, W. Hao, Z. Lin, J. Yao, Y. Wu, *J. Solid State Chem.* **2013**, *205*, 129 – 133.
[38] H. Li, J. Kim, T. L. Groy, M. O'Keeffe, O. M. Yaghi, *J. Am. Chem. Soc.* **2001**, *123*, 4867 – 4868.
[39] Deposition number 2058594 contains the supplementary crystallographic data for this paper. These data are provided free of charge by the joint Cambridge Crystallographic Data Centre and Fachinformationszentrum Karlsruhe Access Structures service.
[40] T. Sasaki, H. Takizawa, K. Uheda, T. Yamashita, T. Endo, *J. Solid State Chem.* **2002**, *166*, 164 – 170.
[41] C. Wang, X. Bu, N. Zheng, P. Feng, *J. Am. Chem. Soc.* **2002**, *124*, 10268 – 10269.
[42] M. Huang, Y. P. Feng, A. T. L. Lim, J. C. Zheng, *Phys. Rev. B* **2004**, *69*, 054112.
[43] G. Gopal Khan, S. J. Clark, N. R. Bandyopadhyay, *Int. J. Mod. Phys. B* **2010**, *24*, 5487 – 5494.
[44] J. T. S. Irvine, D. C. Sinclair, A. R. West, *Adv. Mater.* **1990**, *2*, 132 – 138.
[45] S. Ohno, T. Bernges, J. Buchheim, M. Duchardt, A.-K. Hatz, M. A. Kraft, H. Kwak, A. L. Santhosha, Z. Liu, N. Minafra, F. Tsuji, A. Sakuda, R. Schlem, S. Xiong, Z. Zhang, P. Adelhelm, H. Chen, A. Hayashi, Y. S. Jung, B. V. Lotsch, B. Roling, N. M. Vargas-Barbosa, W. G. Zeier, *ACS Energy Lett.* **2020**, *5*, 910 – 915.
[46] J. Fleig, J. Maier, *J. Am. Ceram. Soc.* **1999**, *82*, 3485 – 3493.

Manuscript received: January 25, 2021
Revised manuscript received: March 4, 2021
Accepted manuscript online: March 18, 2021
Version of record online: May 7, 2021

